

Inertial Response and Power Oscillation Damping Using Fuzzy Controller with Pmsg-Based Wind Turbines

M. Srirekha & Dr. R. Somanatham

M. Tech Student, Department of EEE, CVSR, Hyderabad, Telangana, India
sri.pragna7@gmail.com

Professor, Dept of EEE, CVSR, Hyderabad, Telangana, India

ABSTRACT- According to this paper we are analysis an improved active power control method for variable speed wind turbine which is used to enhance the inertial response with the damping capability during the transient system. Here we are implementing the fuzzy logic controller for the better performance comparing to the other controller. According to the optimized power point tracking (OPPT) controller we can shift the turbine operating point to the maximum power point tracking (MPPT) curve which control the virtual inertia control (VIC) curves according to the frequency deviation which is used to proposed to release the “hidden” kinetic energy and provide dynamic frequency support to the grid. Fuzzy controller is the most suitable for the human decision-making mechanism, providing the operation of an electronic system with decisions of experts. According to the effects of the VIC on power oscillation damping capability which is theoretically evaluated. We are comparing the conventional supplementary derivative regulator which is depend upon the inertia control, during transient events it not only provide the fast inertial response but also increase the system damping capability. By using the simulation result we can analysis the inertial response and power oscillation damping function can be obtained in a single controller by the proposed control system.

Index Terms—Frequency support, permanent magnet synchronous generator (PMSG), power oscillation damping, variable speed wind turbine, virtual inertia control (VIC),fuzzy controller.

I. INTRODUCTION

In recent years, the reduced inertial response and power damping capability, as the result of increased wind power penetration in ac networks, have been receiving considerable attention from wind turbine manufactures and system operators. Tackling these issues requires not only fault ride through capability of the wind turbines, but also the ability to participate in frequency and power regulation during system disturbances so as to make the wind farms grid-friendly power generation sources. Thus, the control potential of variable speed wind turbines need be further explored to ensure the stability of power networks containing large-scale wind energy. This

can be critical for weak power systems containing large scale wind farms, as damping from synchronous generators may be insufficient and active contribution from wind farms becomes essential. At present, auxiliary controllers with frequency feedback are introduced to wind turbines to provide system frequency response, such as P/f droop controller, PD controller, and de loading controller by shifting the maximum power point tracking (MPPT) curves. However, the P/f droop controller equipped in the blade pitch control system can only emulate the primary frequency response.

While the PD controller of the converter employs a df/dt term to emulate additional inertia in the initial frequency change period, the power tracking curve is shifted from the MPPT curve to the right suboptimal curve to provide dynamic frequency support for the grid during a frequency event. However, a smooth recovery to the MPPT operation cannot be realized by these control approaches. Moreover, the damping capabilities of these controllers during grid disturbance are not analyzed. The traditional PSS has been introduced to the DFIG to damp power system oscillations but no frequency support was considered. For all the work reported, simultaneous inertia and damping control cannot be achieved.

II. CONTROL OF PMSG

The proposed inertia and damping control methods are developed considering the power regulation of PMSG-based wind turbine. The dynamic model of the PMSG and associated converters can be found. The electromagnetic power of the generator can be controlled using either the generator-side converter or the grid-side converter. In this paper, the grid-side converter directly controls the generated active power, whereas the generator-side converter is used to maintain a constant dc-link voltage, as seen in Fig. 1. Since the grid-side converter can fall into current limit during ac voltage

dip with reduced power transmission, the generator side converter as the dc voltage control station automatically reduces power generation in order to maintain a constant dc voltage.

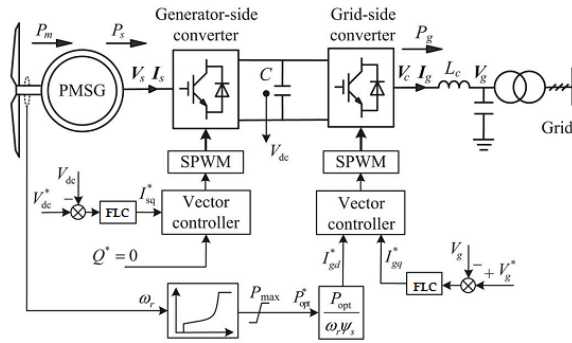


Fig. 1: Schematic control diagram of a PMSG-based wind turbine

The surplus power in the turbine during such disturbances is stored as the kinetic energy of the large rotating masses but only results in a relatively small speed fluctuation of the PMSG. If required, the acceleration of generator speed can be limited using the pitch control to prevent it from going above its rated value. Therefore, the wind turbines do not naturally respond to frequency change or provide power system oscillation damping. It needs to be noted that the ability for a wind turbine to provide inertia support and damping is based on the condition that the wind turbine and associated generator and converter system have the spare power capability. This means that prior to the network disturbance; the wind turbine is operating at below rated power, which is usually the case, as wind turbines are usually only partially loaded.

III. VIRTUAL INERTIA CONTROL OF VARIABLE-SPEED WIND TURBINES

A. Principle of Virtual Inertia Control (VIC)

The inertia constant H_{tot} of a power system with synchronous generators and variable speed wind turbines can be expressed as

$$H_{tot} = \left[\sum_{i=1}^m \left(\frac{J_{s,i} \omega_e^2}{2p_{s,i}^2} \right) + \sum_{j=1}^n E_{w,j} \right] / S_N \quad (1)$$

Where, m and n are the numbers of connected synchronous generators and wind turbines in the grid, respectively. $p_{s,i}$ and $J_{s,i}$ are the numbers of pole pairs and moment of inertia for synchronous generator i , respectively. $E_{w,j}$ is the effective kinetic energy of the wind turbine available to the power

system. S_N is the total nominal generation capacity of the power system.

This can have significant implications for power system operation and could lead to large frequency deviation. The mechanical characteristics of a wind turbine generator can be expressed as

$$\begin{cases} P_m - P_e = J \omega_r \frac{d\omega_r}{p\omega_s^2 dt} \\ J_{vir} = J \omega_r \frac{d\omega_r}{(\omega_r d\omega_s)} \end{cases} = \frac{J \omega_r d\omega_r}{\omega_s d\omega_s} \times \frac{\omega_s d\omega_s}{p\omega_s^2 dt} = J_{vir} \omega_s \frac{d\omega_s}{p\omega_s^2 dt} \quad (2)$$

Where, ω_r is the rotor electrical angular speed and p is the number of pole pairs of the wind turbine generator. P_m and P_e are the mechanical and electromagnetic powers of the wind turbine, respectively. J is the combined natural inertia of the wind turbine generator. J_{vir} is defined as the virtual inertia of the wind turbines.

If the wind turbine is controlled to provide dynamic support using its kinetic energy during a frequency change, the released kinetic energy ΔE_k can be obtained from (2) as

$$\Delta E_k = \int (P_m - P_e) dt = \int (J_{vir} \omega_s / p\omega_s^2) d\omega_s \quad (3)$$

If the converter controls J_{vir} to be constant by adjusting the rotor speed and to move away from the MPPT point, the effective kinetic energy of the wind turbine compared with asynchronous generator can be expressed as

$$E_w = (1/2) J_{vir} (\omega_e / p\omega_s)^2 \quad (4)$$

According to (1) and (4), the inertia constant H_{tot} of the power system with synchronous generators and wind turbines can be expressed as

$$H_{tot} = \left[\sum_{i=1}^m \left(\frac{J_{s,i} \omega_e^2}{2p_{s,i}^2} \right) + \sum_{j=1}^n \left(\frac{J_{vir,j}}{2p_{\omega,j}^2} \right) \right] \omega_e^2 / S_N \quad (5)$$

Where, $p_{w,j}$ and $J_{vir,j}$ are the numbers of pole pairs and virtual inertia for wind turbine j , respectively. It can be seen from (3) that the kinetic energy of the wind turbine can be utilized for inertial response by regulating the generated power, and the equivalent inertia of the wind turbine can be described as

$$\begin{cases} J_{vir} = \frac{J_w \omega_r d\omega_r \Delta \omega_r}{\omega_s d\omega_s \Delta \omega_s} \cdot \frac{\omega_{ro}}{\omega_e} J_w = \lambda \frac{\omega_{ro}}{\omega_e} J_w \\ \lambda = \frac{\Delta \omega_r}{\Delta \omega_s} = \frac{\omega_e}{\omega_0} \times \frac{J_{vir}}{J_w} \end{cases} \quad (6)$$

Where, $\Delta \omega_s$ and $\Delta \omega_r$ are the changes of the grid and rotor angular speed during a frequency event, respectively, λ is defined as the virtual inertia

coefficient, and ω_0 is the pre disturbance rotor speed.

It can be observed from (6) that the virtual inertia of the wind turbine is determined not only by its natural inertia, but also by the pre disturbance rotor speed ω_0 and the virtual inertia coefficient λ .

B. Supplementary derivative control

As proved in (2) and (6), the generated power of the PMSG can be controlled according to the grid frequency deviation to emulate inertial response. The auxiliary power reference P_f^* can be derived from (2) as

$$P_m - P_e = P_m - (P_{opt}^* - P_f^*) \approx P_f^* = J_{vir}(\omega_s d\omega_s / p_w^2 dt) \quad (7)$$

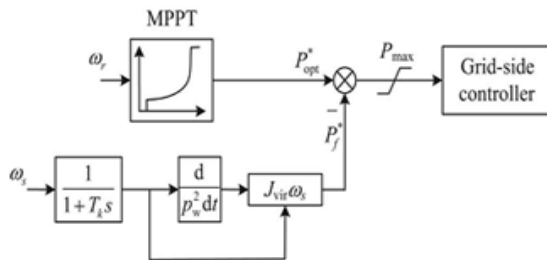


Fig. 2: Block diagram of wind turbine inertia response

Thus, the virtual inertia can be emulated using a supplementary control loop in addition to the normal MPPT controller. Fig. 2 shows the principles of such wind turbine inertia response for system frequency support, and similar schemes have also been investigated in previous research and tested in variable speed wind turbines.

C. OPPT Control for the Inertial Response

In order to achieve better inertia response, the above described interaction between the supplementary inertia control and the MPPT control must be avoided. The VIC proposed in this paper is based on the optimized power point tracking (OPPT) method. When system frequency deviation is detected, the generated power is regulated rapidly by switching the turbine operating point from the MPPT curve to the defined VIC curves. The generated power based on the conventional MPPT control can be expressed as

$$P_{opt}^* = \begin{cases} k_{opt} \omega_r^3 & (\omega_0 < \omega_r < \omega_1) \\ \frac{(P_{max} - k_{opt} \omega_r^3)}{(\omega_{max} - \omega_1)} & (\omega_r - \omega_{max}) + P_{max} & (\omega_1 < \omega_r < \omega_{max}) \end{cases} \quad (8)$$

Where, k_{opt} is defined as the MPPT curve coefficient and ω_0 is the cut-in angular speed. To avoid an abrupt power change around the maximum speed ω_{max} , a droop characteristic of $P - \omega$ is used for the constant speed stage, and ω_1 is the initial angular speed in this stage. P_{max} is the maximum active power output of the PMSG.

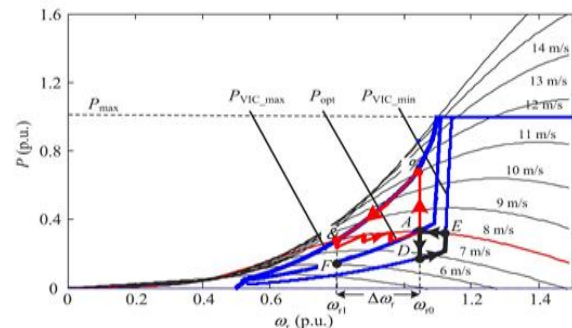


Fig. 3: Scheme of the VIC-based power point tracking curve

$P - \omega$ is used for the constant speed stage, and ω_1 is the initial angular speed in this stage. P_{max} is the maximum active power output of the PMSG. From (8), it can be observed that different curve coefficients will generate a series of power tracking curves, defined as VIC curves. Thus, the regulation of the PMSG's operation point can be achieved by moving it from the MPPT curve with coefficient k_{opt} to the VIC curve with coefficient k_{VIC} .

The rotor speed at point C (ω_{r1}) can be expressed using the frequency deviation as

$$\omega_{r1} = \omega_{r0} + \Delta\omega_r = \omega_{r0} + \lambda\omega_s = \omega_{r0} + 2\pi\lambda\Delta f \quad (9)$$

If the wind speed remains constant, the captured active power at point A can be considered to be similar to that at point C for small rotor speed range. Thus, the VIC curve coefficient k_{VIC} can be calculated as

$$k_{VIC} = [\omega_{r0}^3 / (\omega_{r0} + 2\pi\lambda\Delta f)^3] k_{opt} \quad (10)$$

According to (10), the VIC curve coefficient k_{VIC} is the function of the frequency deviation and replaces the constant coefficient k_{opt} of the MPPT curve. As illustrated in Fig. 3, in the event of a frequency drop, the dynamic response of the VIC can be divided into two stages: 1) fast dynamic frequency support stage (A \rightarrow B \rightarrow C) and 2) slow rotor speed recovery stage (C \rightarrow A). According to (8) and (10), the corresponding power reference curve will then be shifted from P_{opt} to P_{vic_max} and the turbine's operating point is shifted from A to B with its output power changed from P_A to P_B . Since the generated power is greater than the captured mechanical power,

the rotor decelerates and the operating point moves along the P_{vic_max} curve to the operating point C. Consequently, the kinetic energy stored in the rotating mass is released to support the grid frequency response. After the initial dynamic frequency response, the frequency gradually tends to stabilize with the power system's primary frequency regulation. If the power reference curve is switched from P_{vic_max} to P_{opt} directly, a large power step from PC to PF will be injected to the grid, which may result in further frequency oscillation during this recovery progress. However, using the proposed VIC method, the power reference curve will recover to MPPT curve gradually according to (10).

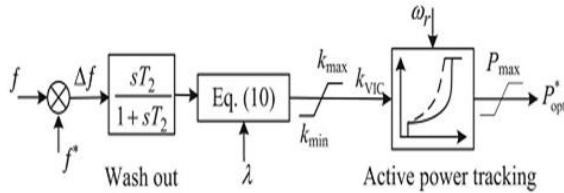


Fig. 4: Structure diagram of the OPPT regulator-based VIC

Fig. 3 shows a special case where the recovery progress from C to A involves switching the operating point from three power reference curves. In reality, the VIC curve coefficient is continuously changed from k_{max} to k_{opt} during the frequency recovery due to the continuous variation of the frequency deviation. Therefore, the rotor speed of the DFIG will smoothly recover to the initial MPPT point. In a similar way, the regulation progress during grid frequency increase can be described as the circle line of $A \rightarrow D \rightarrow E \rightarrow A$ in Fig. 3. In order to ensure wind turbine stability at any wind velocities, the rotor speed needs to be limited within the range $[\omega_{min}, \omega_{max}]$, and the upper and lower limits of the VIC curves (P_{VIC_max} and P_{VIC_min}) can be defined accordingly. Thus, the k_{VIC} calculated by (10) is limited within k_{max} and k_{min} . The block diagram of the OPPT-based VIC is shown in Fig. 4. A wash out filter is used to eliminate the steady-state dc component of the frequency error.

IV. IMPACT OF VIC ON POWER OSCILLATION DAMPING

The equivalent circuit of a three-machine power system, as shown in Fig. 5, is used here for the theoretical evaluation of the effect on damping capability. In Fig. 5, Bus B2 is the swing bus; V_G is the wind farm grid connection point voltage; E is the q-axis transient voltage; V is the terminal voltage

of G_1 ; θ is the phase angle between E and V_G ; δ is the phase angle between E and V ; and δ_0 , θ_0 , and V_G are the initial values of δ , θ , and V_G , respectively. x_1 and x_2 are the line reactance's.

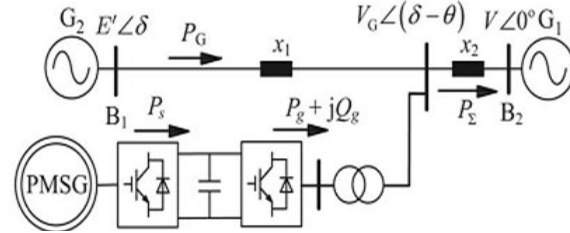


Fig. 5: Equivalent circuit of the power system with wind farms

The active and reactive powers of the synchronous generator G_2

$$P_G = (E'V_G/x_1) \cos \theta - V_G^2 \quad (11)$$

$$Q_G = (E'V_G/x_1) \sin \theta - V_G^2/x_1 \quad (12)$$

The rotor motion equations of G_2 can be written as

$$H_G = (dw_s/dt)P_{Gm} - P_G - D(w_s - w_e) \quad (13)$$

$$\frac{d\delta}{dt} = w_s - w_e \quad (14)$$

Where, H_G , P_{Gm} , P_G , and ω_s are the inertia constant, electromagnetic power, mechanical power, and angular velocity of G_2 , respectively. D is the damping coefficient. Assuming that mechanical power P_{Gm} remains constant throughout the transient process, the rotor motion equations developed by the small perturbation method can be expressed as

$$H_{GP}^2 \Delta \delta + D_p \Delta \delta + \Delta P_G = 0 \quad (15)$$

Where, ΔP_G is the active power variation of G_2 and p is the differential divisor.

In a linear system, the impact of the active power regulation and the grid voltage variation for the system damping can be described by a set of linear ordinary equations, which can be solved, respectively. Thus, the small perturbation quantity of P_G can be obtained as

$$\Delta P_G = (E'V_G/x_1) \cos \theta_0 \Delta \theta \quad (16)$$

A. Supplementary Derivative Control on Power Oscillation Damping

As the auxiliary power reference P_f generated by the supplementary inertial controller fluctuates with the grid power/frequency oscillations, the system damping capability will be changed. As shown in Fig. 5, the network power equation is given by

$$P_\Sigma = P_G + P_g \quad (17)$$

Where, $P = (VGV/x_2) \sin(\delta - \theta)$. Applying small perturbation, the following equation can be derived from (17)

$$[V_G V \cos(\Delta\delta - \Delta\theta)] * (\Delta\delta - \Delta\theta) = \Delta P_G + \Delta P_g \quad (18)$$

Neglecting the small rotor speed variation in the analysis and according to (14), the small perturbation quantity of P_f can be obtained as

$$\Delta P_G = -H_{vir} \left(\frac{d\Delta\omega_s}{dt} \right) = -H_{vir} p^2 \Delta\delta = \Delta P_g \quad (19)$$

The above equation describes the additional power generated by the supplementary controller. Substituting (19) and (16) into (18), $\Delta\theta$ is obtained as

$$\Delta\theta = a_0 \Delta\delta + \left[\frac{H_{vir} a_0 x_2}{(V_G V \cos(\Delta\delta - \Delta\theta))} \right] p^2 \Delta\delta \quad (20)$$

According to the equation which indicates that the eigen value moves toward the right-half plane for increased inertia indicating a reduced damping from the supplementary derivative control.

B.OPPT Control

For the proposed OPPT control, according to (10), the output power of the PMSG can be expressed as

$$P_g = \left[k_{opt} \omega_{r0}^3 / (\omega_{r0} + \lambda(\omega_s - \omega_e))^3 \right] \omega_r^3 \quad (21)$$

During power oscillations, the regulation of P_g mainly depends on the variation of coefficient k VIC. Neglecting the small rotor speed variation, the small perturbation quantity of P_g can be obtained as

$$\Delta P_g \approx - \frac{3\lambda k_{opt} \omega_{r0}^6}{[\omega_{r0} + \lambda(\omega_{s0} - \omega_e)]^4} \Delta\omega_s \approx -3\lambda k_{opt} \omega_{r0}^2 \Delta\omega_s \quad (22)$$

Substituting (16) and (23) into (18), $\Delta\theta$ is obtained as

$$\Delta\theta = a_0 \Delta\delta + [3\lambda k_{opt} \omega_{r0}^6 a_0 x_2 / (V_G V \cos(\Delta\delta - \Delta\theta))] p \Delta\delta \quad (22)$$

Thus, the linear differential equations of the rotor motion can be obtained by substituting (22) and (16) into (15) as

$$H_G^2 \Delta\delta + (D + D_p) p \Delta\delta + \left(a_0 E^1 V_G / x_1 \right) \quad (23)$$

According to (23), the system damping is increased from D to $D + D_p$, by the wind turbines fast power regulation.

V. FUZZY LOGIC CONTROLLER

In FLC, essential control activity is dictated by an arrangement of phonetic standards. These standards are controlled by the framework. Since the numerical factors are changed over into semantic factors, scientific displaying of the framework isn't required in FC. The FLC involves three sections: fuzzification, obstruction motor and defuzzification. The FC is described as I. seven fluffly sets for each

info and yield. ii. Triangular enrollment capacities for effortlessness. iii. Fuzzification utilizing consistent universe of talk. iv. Suggestion utilizing Mamdani's, 'min' administrator. v. Defuzzification utilizing the tallness strategy.

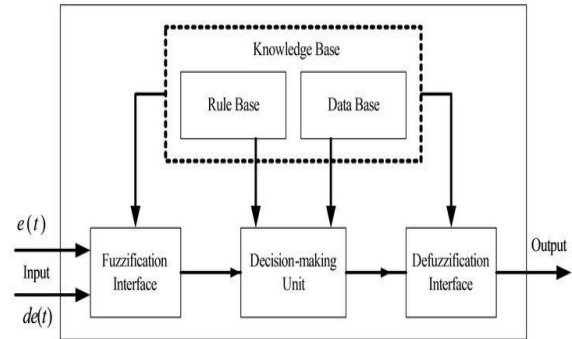


Fig.6: Fuzzy logic controller

TABLE: FUZZY LOGIC CONTROLLER

e \dot{e}	NB	NM	NS	ZE	PS	PM	PB
NB	NB	NB	NB	NB	NM	NS	ZE
NM	NB	NB	NB	NM	NS	ZE	PS
NS	NB	NB	NM	NS	ZE	PS	PM
ZE	NB	NM	NS	ZE	PS	PM	PB
PS	NM	NS	ZE	PS	PM	PB	PB
PM	NS	ZE	PS	PM	PB	PB	PB
PB	ZE	PS	PM	PB	PB	PB	PB

Fuzzification: Enrollment work esteems are doled out to the etymological factors, utilizing seven fluffly subsets: NB (Negative Big), NM (Negative Medium), NS (Negative Small), ZE (Zero), PS (Positive Small), PM (Positive Medium), and PB (Positive Big). The Partition of fluffly subsets and the state of enrollment CE(k) E(k) work adjust the take care of business to fitting framework. The triangular state of the participation capacity of this plan presumes that for a specific E(k) contribution there is just a single predominant fluffly subset. The information blunder for the FLC is given as

$$E(k) = \frac{P_{ph(k)} - P_{ph(k-1)}}{V_{ph(k)} - V_{ph(k-1)}} \quad (24)$$

$$CE(k) = E(k) - E(k-1) \quad (25)$$

Inference Method: A few arrangement strategies, for example, Max- Min and Max-Dot have been proposed in the writing. In this paper Min technique is utilized.

Defuzzification: As a plant more often than not requires a non-fluffly estimation of control, a defuzzification arranges is required. To register the yield of the FLC, „height“ strategy is utilized and the

FLC yield alters the control yield. Further, the yield of FLC controls the switch in the inverter. In UPQC, the dynamic power, receptive power, terminal voltage of the line and capacitor voltage are required to be kept up. To accomplish this, the enrollment elements of FC are: mistake, change in blunder and yield

The set of FC rules are derived from

$$u = -[\alpha E + (1-\alpha) * C] \quad (26)$$

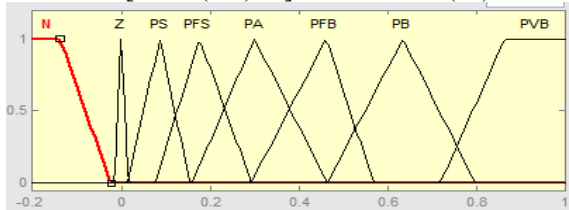


Fig 7: input error as membership functions

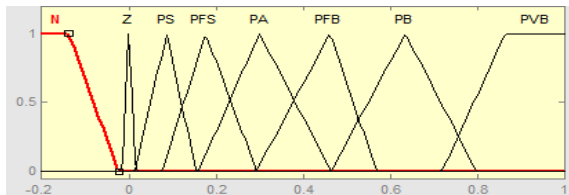


Fig 8: change as error membership functions

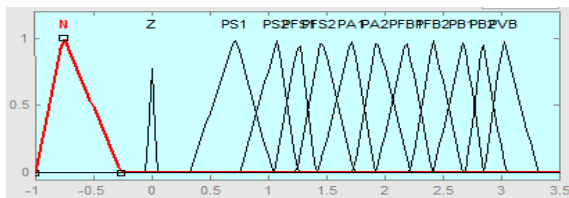


Fig 9: output variable Membership functions

Where, α is self-adjustable factor which can regulate the whole operation. E is the error of the system, C is the change in error and u is the control variable.

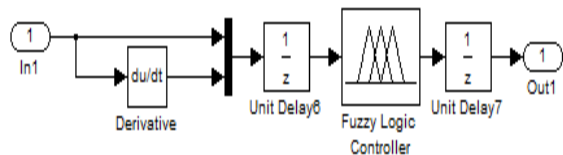


Fig 11: fuzzy logic controller in simulation

VI. SIMULATION RESULTS

The simulation platform is shown in Fig. 6 and consists of two synchronous generators (G1 and G2), a PMSG-based wind turbine with the mechanical turbine and drive chain emulated using a controlled machine set, and three aggregated loads (L1, L2, and L3). G1 and G2 are rated at 15 and 6.8 kVA, respectively.

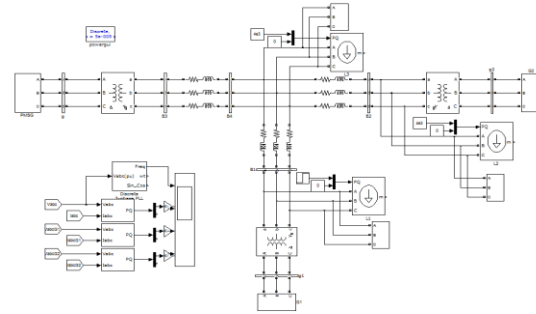
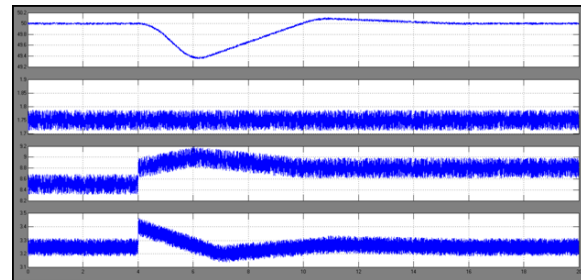


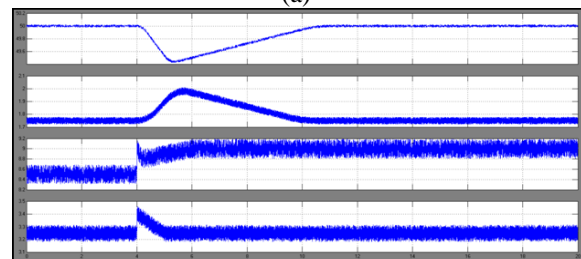
Fig. 12: simulation block diagram of the proposed system

A. Inertial Responses Under Sudden Load Change:

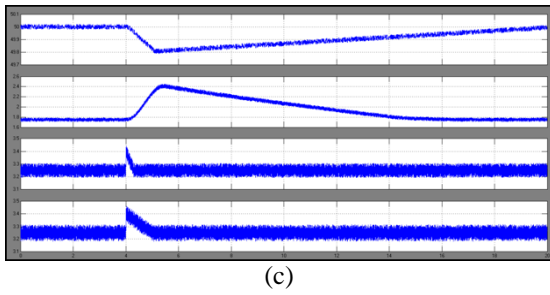
The impact of different virtual inertia coefficients in (10) on the wind turbine inertia response and system frequency is tested first, and the results are shown in Fig. 7. The wind velocity was set as 8 m/s by the motor-based emulator and the PMSG-based turbine initially operated at the maximum power point. During the test, Load L1 was increased from 5.2 to 6.2 kW causing a temporary fall of the system frequency. In Fig. 7(a)–(c), the dynamic responses of the network frequency, the PMSG's active power P_g , G1's active power output $PG1$, and G2's active power output $PG2$ are compared for different control methods and different virtual inertia coefficients λ .



(a)



(b)



(c)

Fig. 13: Dynamic responses of the network during load L1 sudden increase 1 kW. (a) Without VIC. (b) VIC ($\lambda = 1$). (c) VIC ($\lambda = 9$)

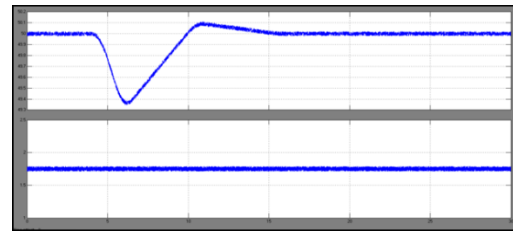
Without the proposed VIC scheme as shown in Fig. 13(a), the active power of the wind turbine remains almost constant at 1.7 kW. A large frequency drop of 0.55 Hz can be observed due to the small system inertia. For the OPPT control scheme, the virtual inertia responses of the PMSG can be regulated by adopting different value of the virtual inertia coefficient λ . The wind turbine switches the control mode from the MPPT control to the VIC control when the frequency deviation occurs. For the results shown in Fig. 13(b) with $\lambda = 1$, the active power of the wind turbine is increased by 0.25 kW and a reduced frequency drop of 0.45 Hz is observed compared to system without VIC. To further increase the virtual inertia of the wind turbine, $\lambda = 9$ is used and the results are shown in Fig. 7(c). It can be seen from Fig. 13(c) that the wind turbine output active power is increased by 0.63 kW, which results in a much smaller frequency drop of 0.21 Hz.

B. Comparison with Supplementary Derivative Control During Load Increase

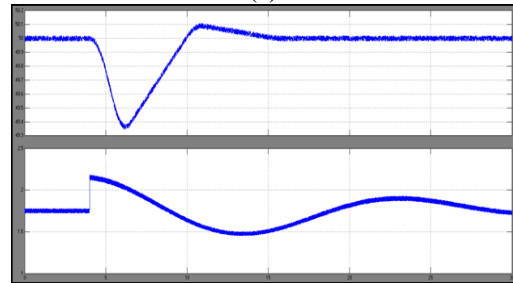
To further illustrate the advantages of the proposed VIC scheme on inertia support and system damping, experimental results are compared for the three cases:

- 1) Case A: without inertia control;
- 2) Case B: with the supplementary derivative control; and
- 3) Case C: with the proposed OPPT control.

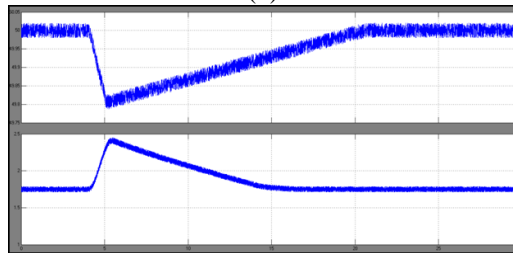
During the tests, L1 was increased from 5.2 to 6.2 kW and the results for the three cases are shown in Fig. 14(a)–(c), respectively.



(a)



(b)



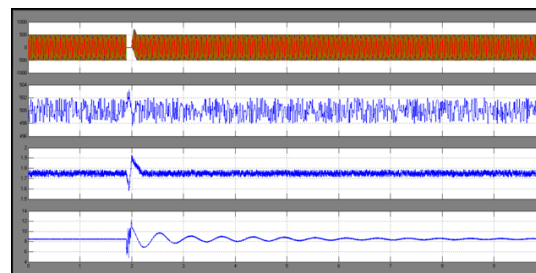
(c)

Fig. 14: Comparison of the inertia response during sudden load increase.

(a) Case A. (b) Case B. (c) Case C.

C. Comparison With Supplementary Derivative Control on Power Oscillation Damping After Short Circuit Fault

In Fig. 15, the ac voltage, the dc-link voltage of the PMSG's converters, the wind turbines' active power, and the active power of G1 are compared under the three same cases illustrated in the previous section. The severity of the three-phase short-circuit fault can be seen from the ac voltage waveforms shown in Fig. 15(a). For case A shown in Fig. 15(a), when the short-circuit fault happens, the grid-side converter goes into current limit



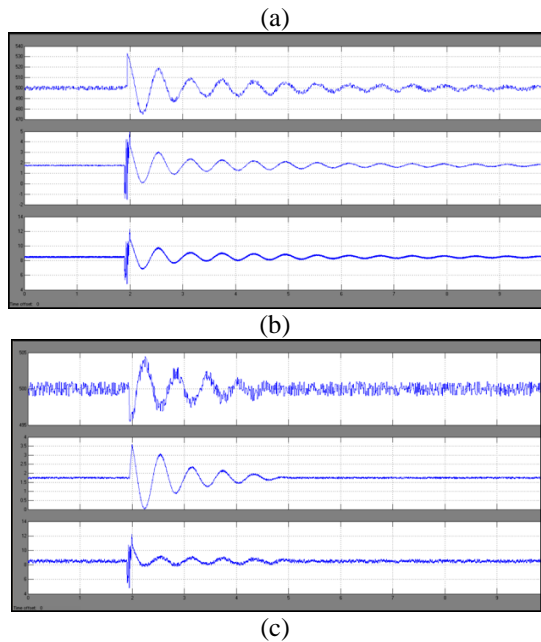


Fig. 15: Dynamic responses of the network after short-circuit fault. (a) AC voltage and Case A. (b) Case B. (c) Case C

As shown in Fig. 15(b) for Case B, the fast active power response from the wind turbine to the network frequency variation is generated by the supplementary derivative controller. Due to the adverse effect of this control resulting in reduced system damping, the system oscillates for a prolonged period after fault clearance. Compared to Case A, the increased dc link voltage and power oscillations can seriously affect the wind turbine operation and grid stability. In Fig. 15(c), with the OPPT control, power oscillations in G1 are significantly reduced.

D. Comparison With Supplementary Derivative Control After Short-Circuit Fault and Load Increase

System operation during a 0.1-s three-phase short-circuit fault at Bus B2 immediately followed by a 1-kW load increase is tested to further illustrate the performance of the proposed OPPT control. The experimental results for the three cases are shown in Fig. 16. Under such test conditions, the initial frequency change and power oscillations are generated by the short-circuit fault. The system frequency then decreases due to load increase. The dynamic response of the network frequency with supplementary derivative control is better than that

with no inertia control as evident from Fig. 16(a) and (b).

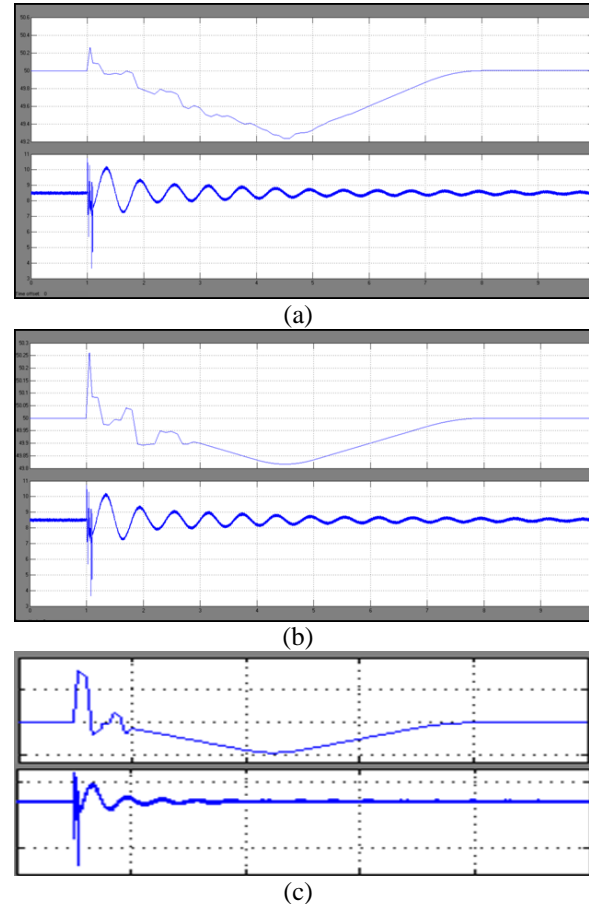


Fig. 16: Dynamic responses of the system after short-circuit fault and load increase. (a) Case A. (b) Case B. (c) Case C

VII. CONCLUSION

In this paper we are implementing a power regulation of PMSG which is depend upon the wind turbine during the transient event to overcome the grid inertial response with the damping capability. Here we are using the fuzzy logic controller for better performance. Here the VIC will depend upon the OPPT of the PMSG which is depend upon the wind turbine will be proposed to provide the inertial response and the power oscillation damping. Therefore the conclusions of this paper from the proposed control method are given below: According to the AC network with the high wind power penetration is such as to decreases the effective inertia and damping capability.

Moreover the wind turbines equipped with virtual inertia and oscillation damping functions become increasingly necessary for ensuring system stability. When we compare with the supplementary derivative control, the proposed OPPT control scheme avoids negative interactions between inertia response and the MPPT control. The OPPT method can change the emulated inertia of the wind turbines by adjusting the virtual inertia coefficient. Different from the supplementary derivative control, OPPT control can also contribute system damping. Thus, the proposed OPPT control scheme for wind turbines has both inertial response and positive damping function, providing an enhanced active power support for improved system stability.

VIII. REFERENCES

- [1] N. Miller and P. E. Marken, "Facts on grid friendly wind plants," in *Proc.IEEE Power Energy Soc. Gen. Meeting*, 2010, pp. 1–7.
- [2] M. Cardinal and N. Miller, "Grid friendly wind plant controls: Wind control-field test results," in *Proc. Amer. Wind Energy Conf.*, 2006, pp.1–8.
- [3] J. Morren, S. de Haan, W. Kling, and J. Ferreira, "Wind turbines emulating inertia and supporting primary frequency control," *IEEE Trans. PowerSyst.*, vol. 21, no. 1, pp. 433–434, Feb. 2006.
- [4] J. Ekanayake and N. Jenkins, "Comparison of the response of doubly fed and fixed-speed induction generator wind turbines to changes in network frequency," *IEEE Trans. Energy Convers.*, vol. 19, no. 4, pp. 800–802, Dec. 2004.
- [5] L. Holdsworth, J. B. Ekanayake, and N. Jenkins, "Power system frequency response from fixed speed and doubly fed induction generator based wind turbines," *Wind Energy*, vol. 7, no. 1, pp. 21–35, Mar.2004.
- [6] A. Mullane and M. O'Malley, "The inertial response of induction machine-based wind turbines," *IEEE Trans. Power Syst.*, vol. 20, no. 3, pp. 1496–1503, Aug. 2005.
- [7] J. G. Slootweg and W. L. Kling, "The impact of large scale wind power generation on power system oscillations," *Electr. Power Syst. Res.*, vol. 67, no. 1, pp. 9–20, Feb. 2011.
- [8] G. Tsourakis, B. M. Nomikos, and C. D. Vournas, "Contribution of doubly fed wind generators to oscillation damping," *IEEE Trans. Energy Convers.*, vol. 24, no. 3, pp. 783–791, Sep. 2009.
- [9] Z. S. Zhang, Y. Z. Sun, and J. Lin, "Coordinated frequency regulation by doubly fed induction

generator-based wind power plants," *IET Renew. Power Gener.*, vol. 6, no. 1, pp. 38–47, Jan. 2012.

- [10] G. Ramtharan, J. B. Ekanayake, and N. Jenkins, "Frequency support from doubly fed induction generator wind turbines," *IET Renew. Power Gener.*, vol. 1, no. 1, pp. 3–9, Mar. 2007.

M.SRIREKHA is currently pursuing M.Tech in ANURAG Group of Institutions (Formerly known as CVSR College of Engineering(Autonomous)) Affiliated to JNTUH, Hyderabad, Telangana, India. She received Bachelor of technology Degree in Electrical and Electronics Engineering from Vignans'institute of management and technology for women Affiliated to JNTU Hyderabad in 2015, and her field of interest includes Power Electronics, electrical Machines and drives control.

Email id: sri.pragna7@gmail.com

DR. R. SOMANATHAM

He is currently working as Professor in EEE DEPARTMENT with Anurag Group of Institutions. He has 35 years of experience in various organizations in teaching.